AGU PUBLICATIONS

JGR

Journal of Geophysical Research: Space Physics

RESEARCH ARTICLE
10.1002/2016JA022532

Key Points:
- Observations of very intense (>1.6 km/s) ion upflow velocities within the cleft ion fountain near 1000 km during quiet times ($Kp < 3$)
- The core ion distributions analysis implies less than 0.3 eV increase in ion temperature, which is consistent with RISR-N observations
- The presence of intense soft electron precipitation and lack of significant ion heating suggest ambipolar electric field as the main driver

Correspondence to:
Y. Shen,
yangyang.shen@ucalgary.ca

Citation:
Shen, Y., D. J. Knudsen, J. K. Burchill, A. Howarth, A. Yau, R. J. Redmon, D. M. Miles, R. H. Varney, and M. J. Nicolls (2016), Strong ambipolar-driven ion upflow within the cleft ion fountain during low geomagnetic activity, *J. Geophys. Res. Space Physics*, *121*, 6950–6969, doi:10.1002/2016JA022532.

Received 13 FEB 2016
Accepted 27 JUN 2016
Accepted article online 6 JUL 2016
Published online 19 JUL 2016

Strong ambipolar-driven ion upflow within the cleft ion fountain during low geomagnetic activity

Yangyang Shen[1], David J. Knudsen[1], Johnathan K. Burchill[1], Andrew Howarth[1], Andrew Yau[1], Robert J. Redmon[2], David M. Miles[3], Roger H. Varney[4], and Michael J. Nicolls[4]

[1]Department of Physics and Astronomy, University of Calgary, Calgary, Alberta, Canada, [2]National Centers for Environmental Information, Boulder, Colorado, USA, [3]Department of Physics, University of Alberta, Edmonton, Alberta, Canada, [4]SRI International, Menlo Park, California, USA

Abstract We investigate low-energy (<10 eV) ion upflows (mainly O^+) within the cleft ion fountain (CIF) using conjunctions of the Enhanced Polar Outflow Probe (e-POP) satellite, the DMSP F16 satellite, the SuperDARN radar, and the Resolute Bay Incoherent Scatter Radar North (RISR-N). The SEI instrument on board e-POP enables us to derive ion upflow velocities from the 2-D images of ion distribution functions with a frame rate of 100 images per second, and with a velocity resolution of the order of 25 m/s. We identify three cleft ion fountain events with very intense (>1.6 km/s) ion upflow velocities near 1000 km altitude during quiet geomagnetic activity ($Kp < 3$). Such large ion upflow velocities have been reported previously at or below 1000 km, but only during active periods. Analysis of the core ion distribution images allows us to demonstrate that the ion temperature within the CIF does not rise by more than 0.3 eV relative to background values, which is consistent with RISR-N observations in the *F* region. The presence of soft electron precipitation seen by DMSP and lack of significant ion heating indicate that the ion upflows we observe near 1000 km altitude are primarily driven by ambipolar electric fields. DC field-aligned currents (FACs) and convection velocity gradients accompany these events. The strongest ion upflows are associated with downward current regions, which is consistent with some (although not all) previously published results. The moderate correlation coefficient (0.51) between upflow velocities and currents implies that FACs serve as indirect energy inputs to the ion upflow process.

1. Introduction

The presence of heavy ions (mainly O^+) of ionospheric origin in the magnetosphere has been established for several decades [*Shelley et al.*, 1972]. These ions reside in diverse magnetospheric regions [*Johnson et al.*, 1977; *Frank et al.*, 1977; *Lundin et al.*, 1979; *Peterson et al.*, 1981] and are thought to play an important role in the magnetospheric plasma environment [*Chappell*, 1988]. The most important supply comes from narrow regions of the dayside auroral oval and polar cap boundary (dayside cleft), where heavy ions are pumped upward along the magnetic field line and then splashed down dispersively according to the species' masses and energies throughout the entire polar cap [*Lockwood et al.*, 1985a; *Waite et al.*, 1985; *Moore et al.*, 1985; *Horwitz and Lockwood*, 1985]. This process is called the "cleft ion fountain" by *Lockwood et al.* [1985b].

The terms "cleft" and "cusp" call for clarification since they are often used interchangeably without distinction. The first direct observation from the ISIS satellite [*Heikkila and Winningham*, 1971] revealed that the low-altitude cusp or cleft region is characterized by approximately magnetosheath-like plasma (less than 1 keV, with an energy spectrum that often peaks at 100 eV for electrons). Afterward, as explained subsequently in *Heikkila* [1985], the cusp was identified as a more localized region near noon within the broader cleft region. With DMSP F7 crossings, *Newell and Meng* [1989] statistically investigated the plasma characteristics and local time variation of these two regions and suggested that the cusp be defined as a region having more direct access to magnetosheath plasma. Specifically, the cusp has higher plasma number flux, lower average energy, and narrower latitudinal and magnetic local time extents than the cleft. Here based on the locations and particle characteristics observed from the DMSP satellites, our ion upflow observations reside potentially outside the cusp region. However, due to the presence of cusp-like particle precipitation and the signatures of the "cleft ion fountain" phenomena, we adopt the term "cleft" to categorize the region of our observations as near the dayside polar cap boundary around magnetic noon.

Low-energy (0–60 eV) upflowing ions, consisting of major ion species (O^+, H^+, and He^+) within the cleft ion fountain [*Lockwood et al.*, 1985b] were described as "upwelling ions" by *Lockwood et al.* [1985a] and *Moore et al.* [1985] from DE-1 observations at altitudes below 9000 km. Based on a backward trajectory analysis, *Lockwood et al.* [1985b] and *Waite et al.* [1985] found that the majority of these ions originate from a restricted region in the topside ionosphere dayside cleft region, where through a "velocity filter" effect and with antisunward convection, heavier ions spread dispersively over the entire polar cap due to their mass and energy differences [*Moore et al.*, 1985; *Horwitz and Lockwood*, 1985]. A similar dispersion effect seen in ion conic pitch angles from EXOS-D (Akebono) observations was reported by *Knudsen et al.* [1994] at higher altitudes, who invoked the "cusp heating wall" concept characterized by rapid transverse energization of ions at the narrow equatorward edge of the cusp region during high geomagnetic activity. Another common feature of the cleft ion fountain is the spatial colocation of field-aligned currents, soft electron precipitation (electron energies <1 keV) and, more often than not, convection reversals with the upflowing ions. Such correlations have been discussed by *Heelis et al.* [1984], *Lockwood et al.* [1985a], *Waite et al.* [1986], and *Tsunoda et al.* [1989] using DE-1, DE-2, and HILAT data. While these authors agree upon the characteristics of the associated soft electron precipitation and convection reversal, they reported different features in the associated field-aligned current regions. Both *Heelis et al.* [1984] and *Tsunoda et al.* [1989] suggested that upward field-aligned currents are associated with intense upward ion fluxes, albeit with sporadic events occurring in a net downward current region. However, *Lockwood et al.* [1985a] reported that the low-latitude part of upwelling ion events mainly occurred in apparently downward current regions, with some others extending into upward current regions. *Waite et al.* [1986] demonstrated events in which upwelling ions straddled both upward and downward field-aligned current regions. Using DMSP and CHAMP observations, *Kervalishvili and Lühr* [2013] reported strong associations between ion upflow and enhancements in ionospheric electron temperature, neutral density, and small-scale field-aligned currents, which flow in both directions within the broader-scale upflows.

Despite the above research, the picture of the altitude evolution of the upwelling in the cleft ion fountain remains incomplete, especially at altitudes near 1000 km. The characteristics of upflowing ions at different altitudes can shed light on the mechanisms of ion upflow but are significantly limited by the sparse availability of spacecraft measurements as well as by ground-based radars, for which measurements become increasingly challenging above 800 km altitude.

Data from two plasma instruments on DE-1 have been used to study the cleft ion fountain above 2000 km: the energetic ion composition spectrometer (EICS) [*Shelley et al.*, 1981] and the retarding ion mass spectrometer (RIMS) [*Chappell et al.*, 1981]. Based on RIMS data, *Lockwood et al.* [1985a] estimated the O^+ outflow rate to be as much as 10^8 cm^{-2} s^{-1} at 1–3 R_E with a total rate from both hemispheres reaching 10^{25} ions s^{-1}. Similar results have been reported by *Pollock et al.* [1990], who in addition to RIMS used the plasma wave instrument (PWI) and magnetic field data to calculate parallel ion bulk flow velocities (1–10 km/s) at around 2 R_E. Using EICS data, *Yau et al.* [1985] statistically investigated the occurrence morphology of energetic upflowing ions above 100 eV at altitudes above 8000 km and found that the solar flux is the causative factor in the long-term variations of the observed upflowing ions morphology and that the O^+ upflowing ion events have significantly higher occurrence rate in summer than in winter. It should be noted that 1 min or 96 s averages were applied to these data. Also, *Bouhram et al.* [2004] investigated the statistical evolution of transverse ion heating as a function of altitude, which extends from above the topside ionosphere to 5.5 R_E, based on ion data in the cusp/cleft from the Akebono, Interball-2, and Cluster satellites. This study stressed the height-integrated nature of transverse ion heating in the cusp/cleft region below 4 R_E.

For observations below 1000 km, *Loranc et al.* [1991] used the DE-2 ion drift meter (IDM) and retarding potential analyzer (RPA) data to investigate the vertical ion flow velocity profile between 200 km and 1000 km and found that velocities in the range of 100–3000 m/s are a common occurrence and that ion flows were generally upward in the cleft region and downward in the polar cap region. Observations by a similar IDM instrument onboard the HILAT satellite showed upflow velocities as high as 1.6 km/s at 800 km altitude [*Tsunoda et al.*, 1989]. At topside ionosphere altitudes, numerous ground-based radar observations have been conducted and the velocity values were in the range of 100–1000 m/s in the cleft/cusp region [*Endo et al.*, 2000; *Ogawa et al.*, 2000, 2008; *Skjæveland et al.*, 2014]. Also, *Burchill et al.* [2010] observed ion upflow up to 500 m/s using the CUSP-2002 sounding rocket's suprathermal ion imager (SII) data at around 700 km. They found that the upflow correlated positively with the energy flux of precipitating magnetosheath electrons and negatively with DC electric field magnitudes.

Table 1. Altitudinal Observations of Ion Upflow and Outflow

Research	Method	Altitude	Ion Upflow/Outflow
Lockwood et al. [1985a]	(DE-1)RIMS	1–3 R_E	10^8 cm^{-2} s^{-1}
Pollock et al. [1990]	(DE-1)RIMS,PWI	1.5–2 R_E	1–10 km/s
Yau et al. [1985]	(DE-1)EICS	>8000 km	>100 eV
Yeh and Foster [1990]	Millstone Hill ISR	1000 km (subauroral)	>3 km/s
Moore et al. [1996]	(SCIFER)STICS	~1000 km	1–2 km/s(O^+) 3–5 km/s(H^+)
Heelis et al. [1984]	(DE-2)IDM,RPA	900 km(nightside auroral)	1–2 km/s
Tsunoda et al. [1989]	(HILAT)IDM	800 km	~1–1.6 km/s
Burchill et al. [2010]	(CUSP-2002)TII	768 km	~500 m/s
Endo et al. [2000]			
Ogawa et al. [2000, 2008]			
Skjæveland et al. [2014]	ISR(VHF radar)	~500 km	100–1000 m/s
Loranc et al. [1991]	(DE-2)IDM,RPA	200–1000˜km	100–3000 m/s
Fernandes et al. [2016]	(MICA) TII	325 km	~300 m/s

At around 1000 km altitude, few samples have been collected, especially for low geomagnetic activity. Using data from the STICS instrument on board the SCIFER rocket crossing of the cleft, *Moore et al.* [1996] found 1–2 km/s upward bulk flow for O^+ (3–5 km/s for H^+) with transverse heating to around 1 eV at around 1200 km. *Heelis et al.* [1984] reported a nightside event of over 2 km/s and a prenoon event of over 1 km/s ion upflows associated with field-aligned currents, large convection flow gradients, and soft electron precipitation at around 900 km altitude in the auroral zone using DE-2 measurements. *Yeh and Foster* [1990] also reported upflow in excess of 3 km/s at 1000 km in the subauroral region using Millstone Hill incoherent radar data during a disturbed time. Table 1 summarizes the upflowing ion observations reported at different altitudes. While the majority (except for one case in *Moore et al.* [1996] and some cases in *Loranc et al.* [1991]) of the previous studies of ion upflow in the dayside cleft region are made during active periods, our ion upflow study will focus on events during low geomagnetic activity.

The mechanisms driving ion upflow and their relative roles have not been fully established yet, particularly near the topside ionosphere. The potential upflow-driving processes for the cleft ion fountain at and below 1000 km mainly include (1) frictional heating from relative motion between convection ion drifts and neutrals, causing increased ion temperature and plasma scale height, which leads to the expansion of thermal plasma in the topside ionosphere [*Loranc and St.-Maurice*, 1994; *Wilson*, 1994]; (2) soft electron precipitation from the magnetosheath, which enhances the thermal electron temperature, thereby generating an ambipolar electric field that can accelerate heavy ions along the magnetic field line [*Whitteker*, 1977; *Liu et al.*, 1995; *Seo et al.*, 1997]; and (3) transverse ion heating by waves (potentially seeded by velocity-shear-driven instability [*Ganguli et al.*, 1994] or current-driven instability [*Kindel and Kennel*, 1971]) of broadband extremely low frequencies [*André et al.*, 1990; *Norqvist et al.*, 1996; *Knudsen et al.*, 1998] or lower hybrid resonance frequencies [*Roth and Hudson*, 1985; *André et al.*, 1994], followed by subsequent parallel acceleration via the mirror force. The last one preferentially occurs at higher altitudes around and above 2000 km [*André and Yau*, 1997]. Note that for the dayside cleft region, photoelectrons can also elevate the ambipolar electric field in a way that is similar to electron heating by soft electron precipitation [*Tam et al.*, 1995; *Khazanov et al.*, 1997]. Based on FAST satellite observations at 4000 km altitudes, *Strangeway et al.* [2005] found that Poynting fluxes, which mainly dissipate through Joule heating in the ionosphere, and soft electron precipitation can both contribute to the ion outflow during active periods in the dayside cusp region, with soft precipitating electrons having higher correlation with upward ion fluxes. *Moore et al.* [2010] built on the results of *Strangeway et al.* [2005] with a "generalized Jean's escape" model, stressing the importance of convection and soft electron precipitation in driving the upward O^+ flux. Recently, *Fernandes et al.* [2016] have reported observations of upflow velocities of several hundred m/s in the nightside at *F* region altitudes from the MICA sounding rocket measurements. The ion upflow was attributed to ambipolar electric fields, though they did not rule out the frictional heating effect.

In this paper, we examine high-resolution images of core ion distributions to determine ion flow velocities and temperatures with high sensitivity. We argue that, during low geomagnetic activity periods, the observed

large upflow velocities in the dayside cleft region around 1000 km are mainly the result of parallel acceleration from the ambipolar electric field established by the magnetosheath-like soft electron precipitation. Section 2 gives a brief description of the data set used in this study. Section 3 identifies and presents three events. The relationship between ion upflow velocity and field-aligned currents is also investigated in this section. Finally, sections 4 and 5 explain our reasoning to support ambipolar electric fields as the driver of the O^+ ion upflows we observe and summarize our findings.

2. Instrumentation

In this study, high-resolution (100 samples per second (sps)) measurements of ion upflow velocities and temperatures are obtained from the Enhanced Polar Outflow Probe (e-POP) suprathermal electron imager (SEI) [*Knudsen et al.*, 2015]. As the name implies, the SEI is focused primarily on electron measurements; however, for this study it was configured to measure positive ions. Field-aligned currents are from the e-POP magnetic field instrument (MGF) [*Wallis et al.*, 2015]. Electron and ion precipitation data and magnetic field data are provided by the Defense Meteorological Satellite Program (DMSP) satellite (F16) Special Sensor J (SSJ/5) [*Hardy et al.*, 2008; *Redmon*, 2014] and Special Sensor Magnetometer (SSM) [*Rich et al.*, 1987]. Large-scale background patterns of ion convection are available from Super Dual Auroral Radar Network (SuperDARN) measurements [*Ruohoniemi and Baker*, 1998]. Electron density and temperature, vector ion convection velocity, and ion temperature data from the Resolute Bay Incoherent Scatter Radar North (RISR-N) [*Bahcivan et al.*, 2010] also contribute to this study for comparison.

The Enhanced Polar Outflow Probe (e-POP) scientific payload is part of the CASSIOPE satellite, launched from Vandenberg Air Force Base on 29 September 2013, orbiting the Earth in a polar elliptical plane with an inclination of 81°, a perigee of 325 km and an apogee of 1500 km at launch. The satellite is three-axis stabilized and nominally nadir-pointing with an orbital velocity of 7–8 km/s. In order to investigate the properties and mechanisms of polar ion outflow, the CASSIOPE satellite carries several scientific instruments: the magnetic field instrument (MGF), the suprathermal electron imager (SEI), the plasma wave receiver (RRI), an auroral imager (FAI) [*Cogger et al.*, 2015], a neutral mass spectrometer (NMS), and the rapid-scanning ion mass spectrometer (IRM) [*Yau et al.*, 2015]. Magnetic field data from MGF, and ion measurements from SEI (operated in a special ion mode) and IRM are used for this study. Because of telemetry restrictions, e-POP high-data-rate instruments (including the SEI) can only run experiments for limited periods (usually 8–16 min) each day.

Mounted on a 43 cm boom, the cylindrical SEI sensor mainly comprises a hemispherical electrostatic analyzer, a microchannel plane (MCP), and a phosphor screen connected with a charge-coupled device (CCD) by fiber optic components. By controlling the radial electric field between hemispherical electrodes, the SEI can measure either electrons or ions. In this study, it is configured to measure two-dimensional ion distribution functions at a frame rate of 100 images per second, from which the kinetic energy ($\lesssim$25 eV for this study) and arrival angles (field of view spanning 360°) of incoming particles can be derived. Distribution images are 64 pixels in diameter at the highest image resolution (Hi-res mode). In this paper, we use Normal mode and Integration mode, which both generate 32 pixel diameter ion distribution images. A typical ion distribution image is presented in Figure 1, which shows a 1 s average of 100 images of SEI ion-Normal mode data at an altitude of 1156 km in the dayside cleft region. The O^+ ram energy (5 eV) plus the −2.3 V external skin voltage displace the ion signal away from the detector center. Note that the higher energy the incident ions have, the farther away from the image center they will land on the detector. The blue arrow shows the antiram direction, which is approximately perpendicular to the magnetic field direction indicated by the red arrow. Smearing in the CCD readout direction causes the signal blurring seen at low levels on the right side in the image.

Since the along-track ion velocity (of the order of several hundred m/s) is far smaller than the satellite velocity (7–8 km/s), and the satellite ram direction is nearly perpendicular to the local magnetic field direction, ion flow velocity parallel to the geomagnetic field manifests as an angular deflection of the first moment of the ion distribution away from the nominal antiram direction. Once the deflection angle θ is determined from the ion images, the nominally vertical component of the cross-track ion velocity is obtained as follows:

$$V_c = (V_s + V_p) \times \tan\theta \simeq V_s \times \tan\theta \quad (1)$$

where V_c is the cross-track ion velocity, V_s is the satellite ram velocity, V_p is the plasma convection velocity in the antiram direction, and θ is the angle between centroid position and the antiram direction. In this calculation we neglect V_p, which is nominally perpendicular to B and is a few hundred meters per second in

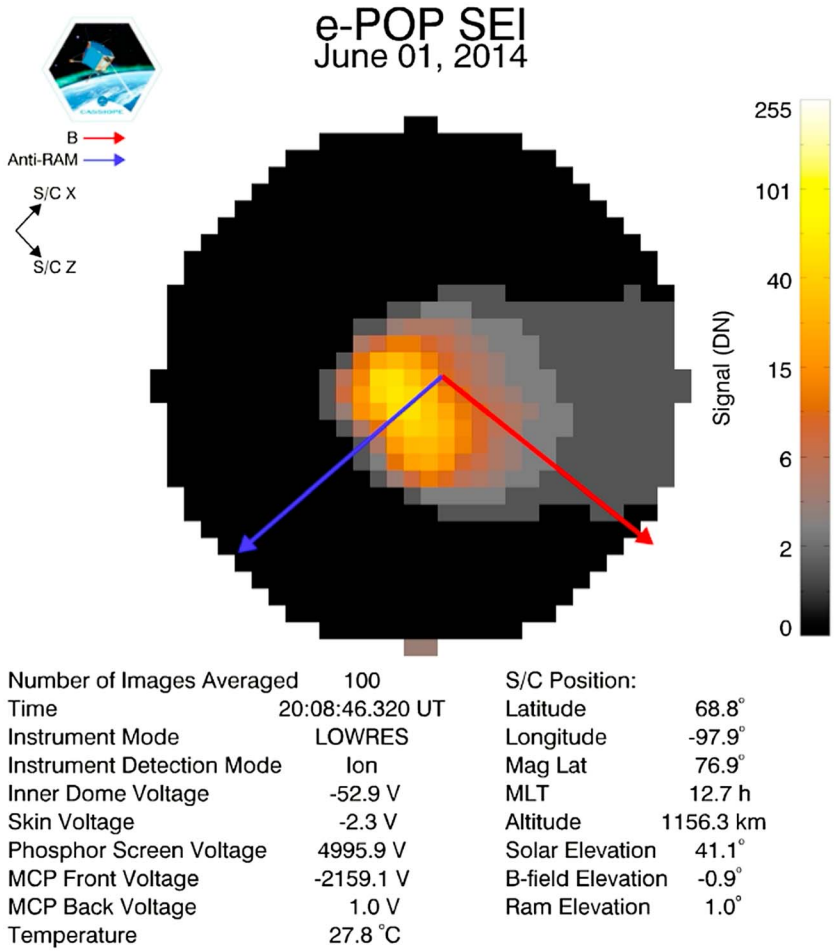

Figure 1. A 1 s average of 100 SEI images in ion mode at an altitude of 1156 km in the dayside cleft region. Ions are preaccelerated by 2.3 V before entering the analyzer; the outer radius maps to an energy of approximately 32 eV. The blue arrow shows the antiram direction, which is approximately perpendicular to the magnetic field direction indicated by the red arrow. Smearing in the CCD readout direction causes the signal blurring seen at low levels on the right side in the image.

our cases, based on SuperDARN and RISR-N observations. In principle, V_p can be obtained directly from the SEI measurements; however, there is an additional error stemming from uncertain knowledge of spacecraft potential, leading us to neglect this component given its secondary effect on V_c. The ion velocity parallel to B can be obtained by projecting V_c onto the magnetic field direction. The resulting ion parallel bulk flow velocity is given in the spacecraft coordinates. As a result of the centroid calculation using many pixels, the angular resolution of the centroid variation is of the order of 0.2°, corresponding to a cross-track velocity resolution of 25 m/s. Note that the SEI is able to measure ion drift velocities with high frame rate (100 sps) and high precision. By comparing rocket-based measurements of ion drifts and $E \times B$ drifts, *Sangalli et al.* [2009] found the uncertainty of ion drift velocity from an SEI-like instrument to be within 16–20 m/s (using a slightly different technique than that used in this paper). In our case, the uncertainty in the cross-track ion velocity, mainly owing to neglect of V_p in equation (1), reaches a maximum of 235 m/s in extreme conditions, when V_p can reach 500 m/s as indicated by ground-based radar data (not shown here) and the angular deviation reaches 25° (corresponding to an ion upflow velocity of 3.3 km/s). And if a total convection velocity up to 1400 m/s, for example, as observed by the RISR-N in one case, completely projects into the along-track direction instead of 323 m/s as observed, the error can reach 650 m/s in the V_c estimate. However, for the majority of cases in our observations, when the angular deviation is less than 10°, the uncertainties are less than 60 m/s for upflow velocities.

We also estimate ion temperatures by determining the distribution function width. Through forward modeling of the ion images with a Monte Carlo charged particle ray tracing simulation [*Burchill et al.*, 2010] adapted to the SEI instrument, we find a linear relation between the distribution's full width at half maximum (FWHM, measured in pixels) and ion temperature (eV) : $T_i = 0.41 \times \mathrm{FWHM} - 1.05$. The ability of the SEI design to detect ion heating in the 1–10 eV range was demonstrated by the GEODESIC sounding rocket [*Burchill et al.*, 2004].

The magnetic field instrument (MGF) [*Wallis et al.*, 2015] on board e-POP samples the magnetic field 160 times per second to a resolution of 0.0625 nT in the spacecraft frame, from which high-resolution (of the order of 100 m) field-aligned current (FAC) structure can be derived through Ampere's law by measuring the perturbed magnetic field gradients along the track of the spacecraft, assuming an infinite current sheet geometry in a plane normal to the satellite velocity. In the events studied in this paper, the spacecraft traverses the cusp from south to north. The field-aligned currents are calculated from the east-west components of the magnetic perturbation gradients along the satellite track. For simplicity, magnetic field perturbations are estimated by subtracting a background field which is approximated by fitting eighth-order polynomials to the undisturbed magnetic field values measured by the MGF. The resulting large-scale DC field-aligned current densities data are calculated in 5 s intervals for comparison with ion upflow measurements.

Data also available for this study are the ion composition measurements from the IRM instrument on e-POP and the precipitating electron (30 eV–30 keV) data from the SSJ/5 instrument onboard the DMSP F16 satellite taken within a few minutes of the e-POP cleft crossings. A detailed description of the IRM instrument can be found in *Yau et al.* [2015]. The DMSP F16 satellite started operations on 28 October 2003. This satellite maintains a Sun-synchronous orbit at an inclination of 98.8°, an orbit period of approximately 101 min, and an altitude of around 850 km. The SSJ/5 instrument on board the satellite measures the electron spectrum from 30 eV to 30 keV in 19 logarithmically spaced energy channels every second. Magnetic field data from SSM are also presented for comparison. The DMSP data are provided and plotted by the National Centers for Environmental Information (NCEI).

The SuperDARN [*Ruohoniemi and Baker*, 1998] is an international network of high-frequency radars located at middle- and high-latitude regions for observing the line-of-sight (LOS) component of ion convection in the *F* region ionosphere. LOS ion drift data are from Rankin Inlet (RKN) and Inuvik (INV) echoes and averaged to a 2 min time resolution, mapped onto Magnetic Local Time (MLT) and Altitude Adjusted Corrected Geomagnetic Coordinates (AACGM).

The RISR-N radar is a northward facing phased-array antenna system, which is electronically steerable for directional spatiotemporal investigations of plasma parameters in the polar cap [*Bahcivan et al.*, 2010]. The 3 min integrated LOS ion velocity, ion temperature, electron density, and temperature data from the five long-pulse beams data are available for this study. The in-track ion velocities along the e-POP orbit derived from the LOS ion velocities [*Heinselman and Nicolls*, 2008] are mainly used to justify our assumption of relatively small plasma drifts in deriving the ion upflow velocity from the SEI.

The three identified cleft ion fountain events are on 30 May, 1 June, and 6 June 2014. In all events, the e-POP satellite went from magnetic local noon near 75° magnetic latitude across the polar cap region into the nightside region in the Northern Hemisphere. The cleft crossings took place at an altitude of approximately 1000 km. On 30 May and 1 June, the DMSP F16 satellite traversed the same region near the cleft 3 min before and 14 min after the e-POP crossing, respectively.

3. Data

3.1. Event 1: 1 June 2014

An intense ion upflow event in the cleft region followed by downward ion flow in the polar cap region was observed by the e-POP satellite on 1 June 2014, from 20:08 to 20:16 UT, at altitudes from 1150 km to 950 km. e-POP stayed in the intense upflow region for about 2 min, corresponding to approximately 900 km along the satellite track. The region spanned magnetic latitudes from 75° to 86° across the cleft and polar cap region. The MLT was near local noon when the large ion upflow velocities were observed, after which e-POP went into the premidnight sector where downward flow was observed.

Figure 2 presents the e-POP (blue line) and the DMSP F16 (green line) satellite orbits and measurements during Event 1 in AACGM latitudes and MLT coordinates. The red lines indicate the upward ion flow region and the blue lines the downward ion flow region (from the perspective of e-POP). The length of the line represents the

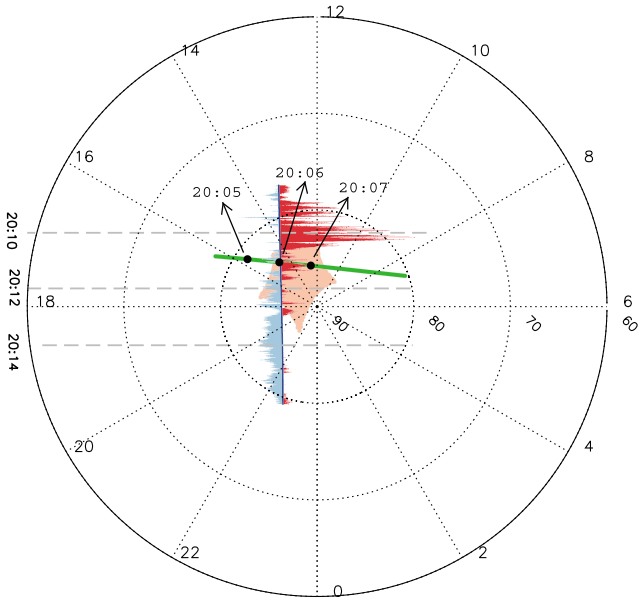

Figure 2. The e-POP (blue line) and the DMSP F16 (green line) satellite orbits and measurements during Event 1 on 1 June 2014 in AACGM latitudes and MLT coordinates. The grey dashed lines indicate the UT for points along the e-POP orbit. The other three times shown (20:05, 20:06, and 20:07 UT) by the black dots represent the close conjunction times of the DMSP F16 satellite. Red and blue lines represent upward and downward ion flow, respectively. The maximum upflow velocity in this event is 1.64 km/s. The upflow region spanned latitudes from 78° to 85° AACGM across the dayside polar cap boundary. The downward ion flow velocities were of the order of 200 m/s relative to values equatorward of the cleft. The salmon polygon region indicates the field of view (FOV) of RISR-N, the data from which demonstrate electron temperature enhancement (over 4000 K, not shown here).

magnitude of the velocity, the maximum value of which in this event is 1.64 km/s. It should be noted that when calculating ion upflow velocity for this event, a baseline value (1100 m/s) was subtracted from the profile. The baseline value was chosen based on the assumption that the ion upflow velocity was small during the minute of observations taken equatorward of the cleft. The upflow region spanned from 78° to 85° across the dayside cleft and into the polar cap region. The downward ion flow velocities were in general about 200 m/s in this figure. The so-called cleft ion fountain feature [*Lockwood et al.*, 1985b], usually observed at several earth radii, is also identifiable at these relatively low altitudes of about 1000 km. From 20:05 to 20:07 UT, the DMSP F16 satellite (green line) traversed the poleward edge of the ion upflow region. The SSJ/5 instrument on board the satellite observed intense fluxes of soft electron precipitation during this close conjunction. IRM observations from e-POP reveal that approximately 90–95% of ions are O^+(mixed with a small amount of N^+ and NO^+ ions), and about 5–10% of ions are H^+ (data not shown here). Also, data from RISR-N reveal lasting electron temperature enhancements (over 4000 K) without ion temperature increases (not shown here).

The *Kp* index value is extremely low in this event (0+). The Interplanetary Magnetic Field (IMF) data were obtained from the OMNI website, which accounts for time shifts resulting from the ACE spacecraft's position 17 R_E upstream of the Earth. For more than 30 min before and throughout this event, the B_y component of the IMF was stable around 4 nT with B_z ranging from −1 to 0 nT. Based on these stable conditions, we assume that the observed upflow structures are spatial rather than temporal features.

Figure 3 presents an overview of this event observed by the e-POP SEI and MGF as a function of UT. Figure 3a shows the ion upflow velocities observed by the SEI. The intense upflow region spans from 20:09 to 20:11 UT, from corrected geomagnetic latitude 77° to about 82°. Figure 3b gives the perpendicular (to B) FWHM variations of the ion distribution functions and therefore the perpendicular thermal ion temperature variations. As mentioned in the previous section, the temperatures have been modeled using a Monte Carlo simulation of the instrument. The FWHM profile shows weak variations (less than 0.7 pixel) in the region of intense ion upflow. These variations indicate weak ion heating in the perpendicular direction with an upper limit of 0.28 eV, which indicates that wave-particle or frictional heating is not contributing to the intense ion upflow seen by e-POP. During active periods the ion heating in the perpendicular direction can be very evident and

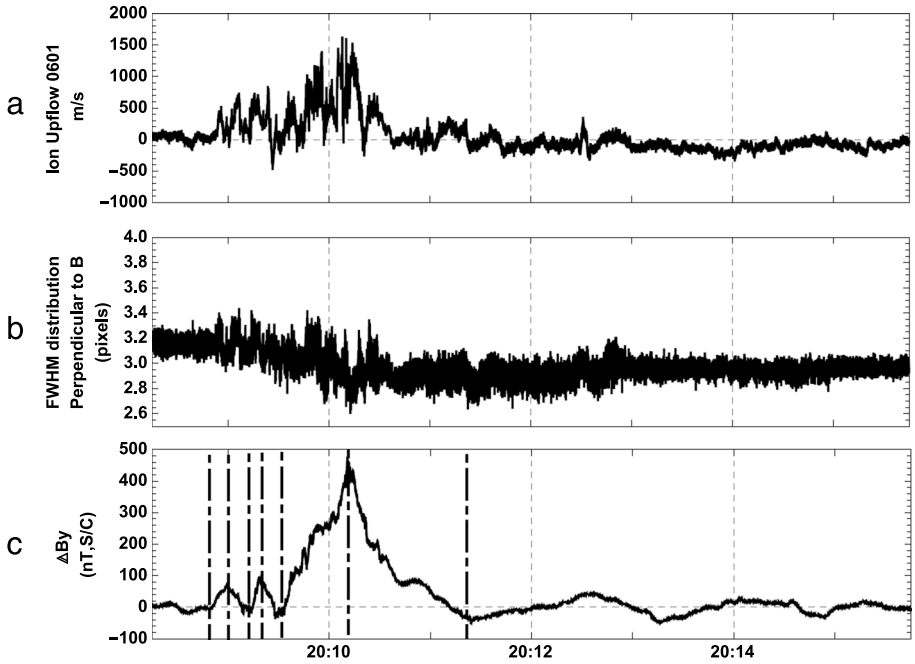

Figure 3. Overview of Event 1 on 1 June 2014 observed by the SEI and the MGF onboard e-POP as a function of UT. (a) The ion upflow velocities observed by the SEI. The intense upflow region spans the periods 20:09 to 20:11 UT. (b) The perpendicular (to B) FWHM variations of the ion distribution functions. The FWHM profile shows weak variations in the region of intense ion upflow, indicating weak ion heating in the perpendicular direction with an upper limit of 0.28 eV. (c) The magnetic field perturbation in the cross-track direction, which is eastward for positive values in this event. The positive gradients of ΔB_y indicate downward current regions, while the negative gradients upward current regions. Six current sheets can be identified between the vertical dash-dotted lines.

intense, such as that reported by *Knudsen et al.* [1998], who demonstrated heating up to tens of eV at 1350 km altitude in the cusp/cleft region.

Figure 3c shows the magnetic field perturbation in the horizontal cross-track direction, which is eastward for positive values in this event. The profile demonstrates that the structured field-aligned currents correlate well with the intense upflow region. The positive gradients of ΔB_y along the satellite track indicate downward current regions, while the negative gradients correspond to upward current regions. Assuming an infinite current sheet structure of the FACs, one can distinguish six current sheets inside this region from the magnetic field perturbation patterns, with the first two pair-of-current sheets having smaller magnitude and latitudinal coverage than the last pair-of-current sheets (shown as the vertical dash-dotted lines). As pointed out by *Lühr et al.* [2015], the infinite current sheet approximation might be compromised near the cusp region, in which case our values underestimate the true magnitudes of the currents. Despite this caveat, this comparison demonstrates that the strongest ion upflows happen in the region of downward currents and that the field-aligned currents correspond well to the intensity of ion upflow velocity, which motivates us to further investigate the relationship between these two in section 4.4.

Figure 4 shows the ion and electron energy flux observations from the SSJ/5 instrument on board the DMSP F16 satellite, along with the magnetic field data for context. Of particular interest is the time period indicated by the rectangular red box. From around 20:05 to about 20:07 UT, intense precipitating electrons and energy fluxes are observed by the SSJ/5 instrument. The peak energy of precipitating electrons first appears to be above 1 keV before 20:05:30, then decreases to less than 1 keV between 20:06 and 20:07:30 UT, and peaks around 200–400 eV, which is the signature of magnetosheath-like soft electron precipitation. The peak energy fluxes exceed 1 mW m^{-2} (1 erg cm^{-2} s^{-1}) as indicated in Figure 4c. From 20:05 to 20:07 UT, the F16 satellite went from AACGM latitude 81° to about 86°, near the magnetic local noon from 15.6 MLT to 12.2 MLT. After about 3 min, the SEI instrument on e-POP observed large ion upflows within and equatorward of the same region.

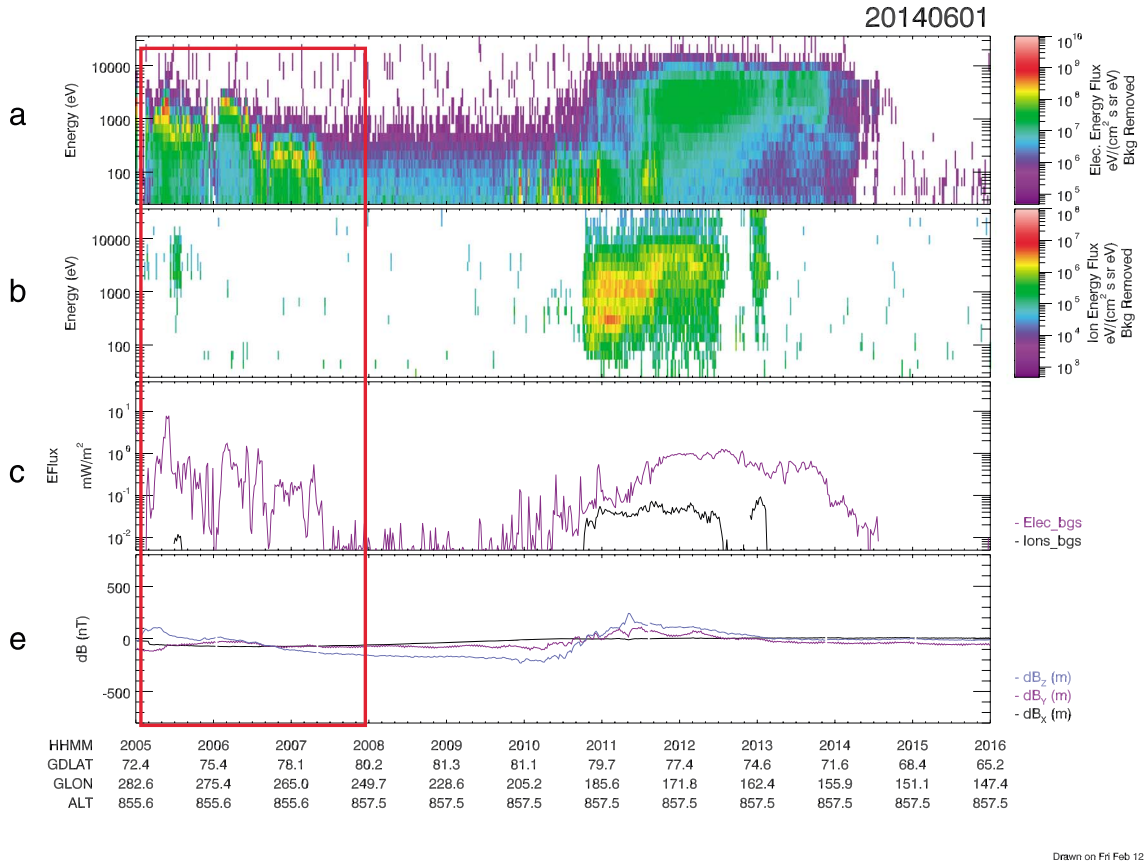

Figure 4. DMSP F16 satellite observations for Event 1. Conjunction time periods with e-POP are indicated within the red rectangular box region. (a, b) Differential energy fluxes for precipitating electrons and ions observed by the SSJ/5 instrument. (c) Integrated electron and ion energy fluxes. The peak energy of precipitating electrons first appears to be above 1 keV before 20:06, then decreases to less than 1 keV between 20:06 and 20:07:30 UT, and peaks around 200–400 eV, which is the signature of magnetosheath-like soft electron precipitation. The total electron energy flux exceeds 1 mW m^{-2} (1 erg cm^{-2} s^{-1}) as indicated in Figure 4c. (d) The magnetic perturbations observed by the magnetometer (SSM).

Figure 4d shows the magnetic perturbations observed by the DMSP magnetic field instrument (SSM). The SSM coordinate frame is defined as follows: $+x$ is positive downward along the local vertical direction, $+y$ is perpendicular to $+x$ in the forward direction of travel and $+z$ is perpendicular to $+x$ and $+y$ and toward the nightside of the orbit plane. Nearly no significant magnetic variations were observed compared to MGF measurements about 3 min later; this can be explained by the fact that the DMSP crossing is in the eastward direction and supports the assumption of current sheets aligned in the E-W direction.

Heelis et al. [1984] and *Tsunoda et al.* [1989] reported correlations of ion drift gradients with ion upflows in the auroral and dayside cleft region. To better understand the environment around ion upflow regions and the field-aligned currents, we also examine the convection pattern observed by SuperDARN during this period. Figure 5 shows the convection map from SuperDARN ion drift measurements. The map is organized according to magnetic latitude and MLT coordinates. A clear two-cell pattern is observed. Ion drift data are available around the magnetic local noon near 80° AACGM latitude. The time window and the location are in general conjugate to large ion upflow observations from the SEI. The e-POP orbit is indicated as a red line when SEI observes large ion upflows. The ion convection velocities are generally eastward with a weak north-south component, which is consistent with our assumption when calculating ion parallel velocity in section 2. There is a clear velocity shear along the satellite orbit, where dawnside flows have larger velocities.

3.2. Event 2: 6 June 2014

Another intense cleft ion fountain event was recorded on 6 June 2014, from 19:49 to 20:05 UT, also at altitudes around 1000 km. During this long period of 16 min, e-POP went from AACGM latitude 65° in the dayside cleft region around 12 MLT, across the polar cap region to a maximum latitude of about 86°. The SEI was

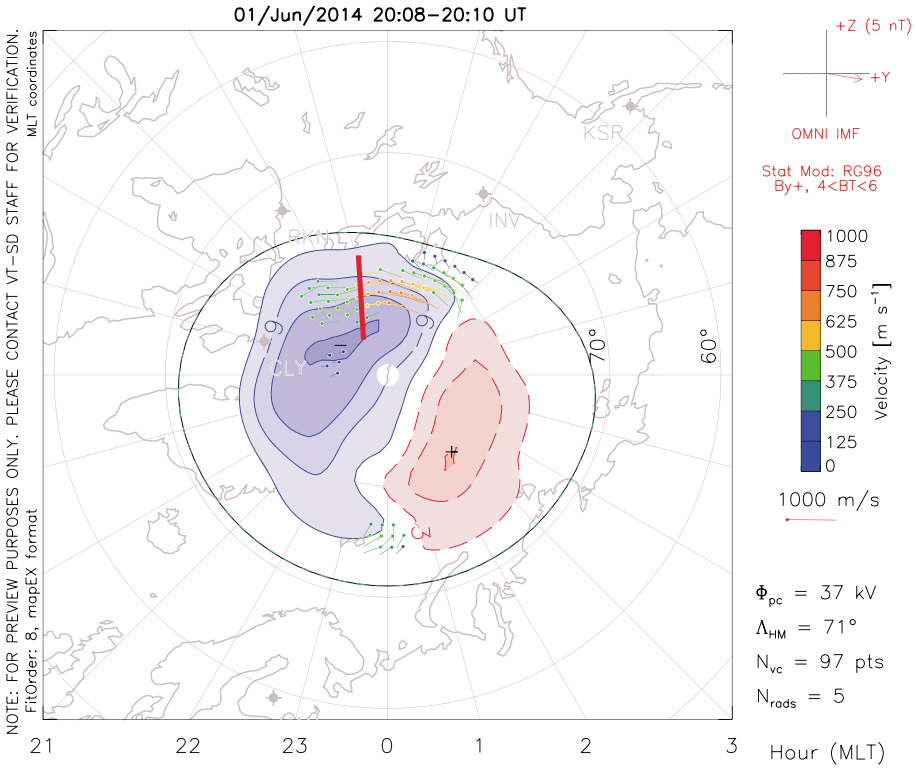

Figure 5. The 2 min averaged convection map from SuperDARN ion drift measurements for Event 1. The map is organized according to magnetic latitude and MLT coordinates. The e-POP orbit is indicated by the red line when SEI observes large ion upflow. The ion convection velocities are generally eastward. There is a clear velocity shear along the satellite orbit, where dawnside flows have larger velocities.

running in ion integration mode, which conserves telemetry bandwidth through software binning both in pixels (32 pixels in diameter) and in time (averaging to 10 images per second) in this case.

Figure 6 displays the overview of Event 2 as well as the e-POP satellite orbit in the same manner as in the previous section. The grey dashed lines specify the time span of the e-POP spacecraft orbit from about 19:50 to 20:05 UT, within which from 19:54 to 19:56 UT the SEI again observed intense ion upflow in the cleft region (red line spikes) followed by large regions of downflow ions across the polar cap (blue line regions). In this case a baseline value of 800 m/s is subtracted from the profile. The largest ion upflow velocity reaches 1.72 km/s and the largest ion downflow velocity immediately adjacent to the upflow region is about 0.8 km/s. The fountain feature is again clearly evident in this event. The *Kp* value is 2− in this event. For 20 min from 19:40 to 20:00, the IMF B_y is stable around −5 nT and B_z around 0 nT. The conjunctional RISR-N radar FOV are inside the polar cap region.

Figure 7 summarizes the observations from the SEI and the MGF onboard e-POP for Event 2 in the same form as Event 1. Figure 7a displays the ion upflow velocity profile as shown in Figure 6. The strong ion upflow region spans 2 min, corresponding to a spatial scale of around 900 km along the satellite orbit, which is similar to Event 1. The downflow region is broader, across the entire polar cap and into nightside region. Mass and energy dispersion associated with the "velocity filter effect" driven by antisunward convection could explain the large spatial coverage of downflowing ions [*Lockwood et al.*, 1985b; *Horwitz and Lockwood*, 1985; *Moore et al.*, 1985].

Figure 7b displays the perpendicular-to-B FWHM profile of the ion distribution functions and shows weak variations in the region of intense ion upflow. In this case the variations in FWHM (less than 0.4 pixel) are larger than those seen in Event 1 and indicate some heating with an upper limit of 0.16 eV. Figure 7c shows the magnetic field perturbation in the horizontal (east-west) direction, which represents a sandwich-like structure consisting of three current sheets (indicated between the dash-dotted lines), with downward currents preceding strong ion upflow and followed by large upward currents and another downward current region.

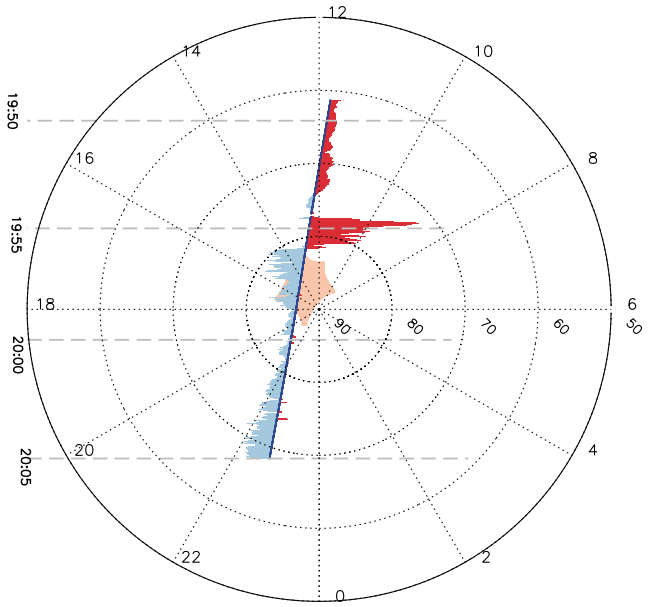

Figure 6. The e-POP satellite orbit and measurements during Event 2 on 6 June 2014 in the same manner as in Event 1. The grey dashed lines specify the time span of the e-POP spacecraft orbit from about 19:50 to 20:05 UT, within which from 19:54 to 19:56 UT, the SEI again observed intense ion upflow in the cleft region (red line spikes) followed by large regions of downflow ions across the polar cap (blue line region). In this case a baseline value of 800 m/s is subtracted from the profile. The largest ion upflow velocity reaches 1.72 km/s, and the largest ion downflow velocity immediately adjacent to the upflow region is about 0.8 km/s.

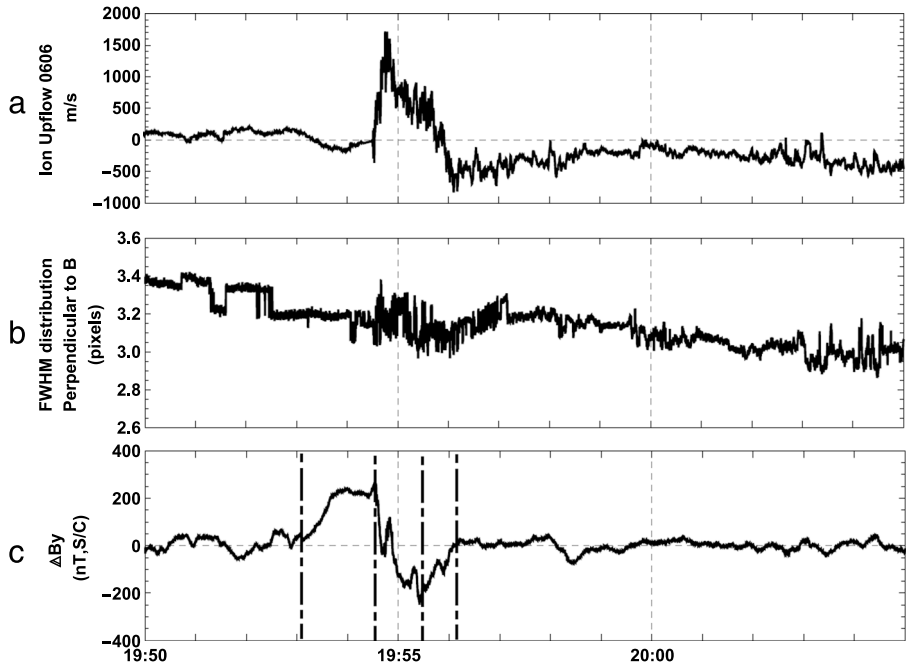

Figure 7. Overview of the SEI and the MGF observations for Event 2 on 6 June 2014 in the same format as in Event 1. (a) The ion upflow velocity profile. The strong ion upflow region spans 2 min. The downflow region is broader, across the entire polar cap and into nightside region. (b) The perpendicular-to-B FWHM profile of the ion distribution functions and shows weak variations in the region of intense ion upflow. In this case the variations in FWHM indicate some heating with an upper limit of 0.16 eV. Note that the discontinuities at the start of the observations are not real. (c) The magnetic field perturbation in the horizontal (east-west) direction, which represents a sandwich-like structure consisting of three current sheets (indicated between the dash-dotted lines), with downward current preceding strong ion upflow and followed by large upward currents and another downward current region. There were also small and localized current sheets embedded within these large-scale currents.

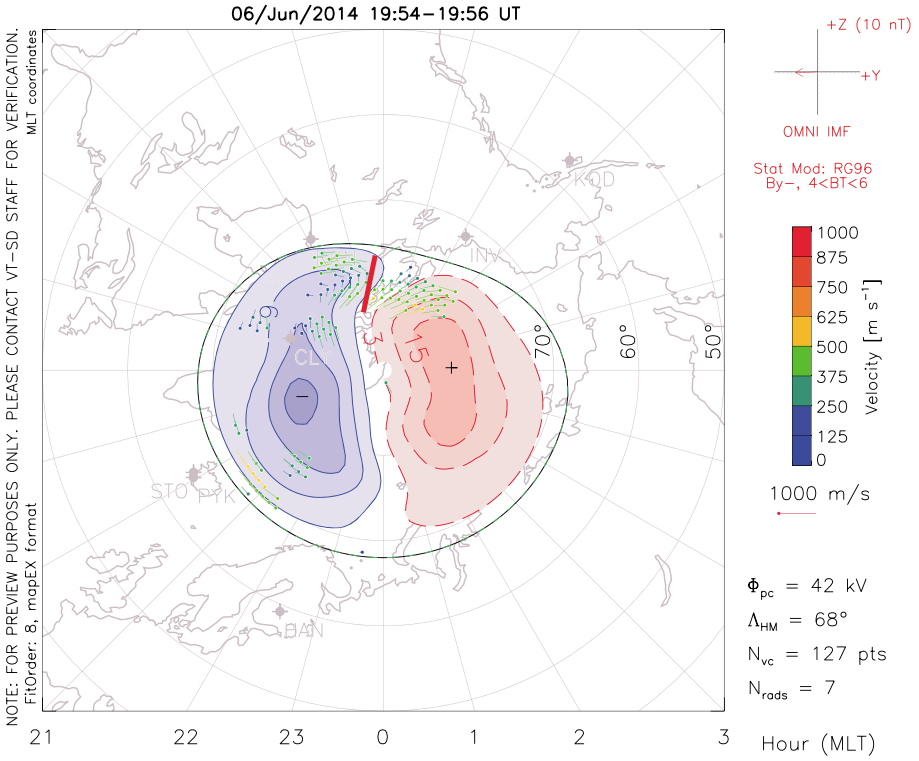

Figure 8. The 2 min averaged convection map from SuperDARN ion drift measurements for Event 2 on 6 June 2014, in the same format as Figure 5. The time span of the convection measurement is from 19:54 to 19:56 UT in conjunction with the SEI upflow observations. The twin-cell pattern is clearly identifiable with antisunward flow of 500–600 m/s around magnetic local noon. The most prominent feature in this figure is the half vortex convection region in the vicinity of the intense ion upflow region, indicated by the red line near 80° AACGM latitude near magnetic local noon. The ion convection was generally antisunward along the orbit with a region of reversal in the zonal flow from eastward to westward. This is consistent with the upward currents observed by e-POP MGF in the ion upflow region.

There were also small and localized current sheets embedded within these large-scale currents. Most of the ion upflow region lies within the large-scale upward current region, while it is also interesting to note that the most intense ion upflow happened in the small downward current sheet region as indicated by the first small spike in the large negative magnetic perturbation gradient region. The IRM data are also available for this event but not shown here. Again O^+ ion was the dominant (90%) ion species with a fraction of H^+ (10%).

Figure 8 displays the ion convection data from SuperDARN observation in this event. The time span of the convection measurement is from 19:54 to 19:56 UT in conjunction with the SEI upflow observations. The twin-cell pattern is clearly identifiable with antisunward flow of 500–600 m/s around magnetic local noon. These antisunward velocities are in general larger than in Event 1 and might result in overestimation of ion upflow velocities in this case, but with errors that remain small relative to the overall upflow velocities (less than 8%). The most prominent feature in this figure is the half vortex convection region in the vicinity of the intense ion upflow region, near 80° AACGM latitude near magnetic local noon. The ion convection was generally antisunward along the orbit (indicated by the red line) with a region of reversal in the zonal flow from eastward to westward. This is consistent with the upward currents observed by e-POP MGF in the ion upflow region.

3.3. Event 3: 30 May 2014

The strongest event took place on 30 May 2014, with e-POP, DMSP F16 satellite, SuperDARN, and RISR-N measuring the region of interest. An overview of the observations from the e-POP SEI is presented in Figure 9. From 21:58 to 22:06 UT, e-POP went from 78° magnetic latitude in the dayside cleft near 13 MLT into the polar cap and nightside region, reaching a maximum geomagnetic latitude of 88°. The altitudes were from 1150 km to 1050 km. Right after the experiment began, from 21:58 to 22:01, the SEI encountered very large ion upflow velocities up to 3 km/s around the polar cap boundary after magnetic local noon. It should be noted that the ion data are integrated to 0.1 s to calculate the vertical cross-track velocities. The subtracted

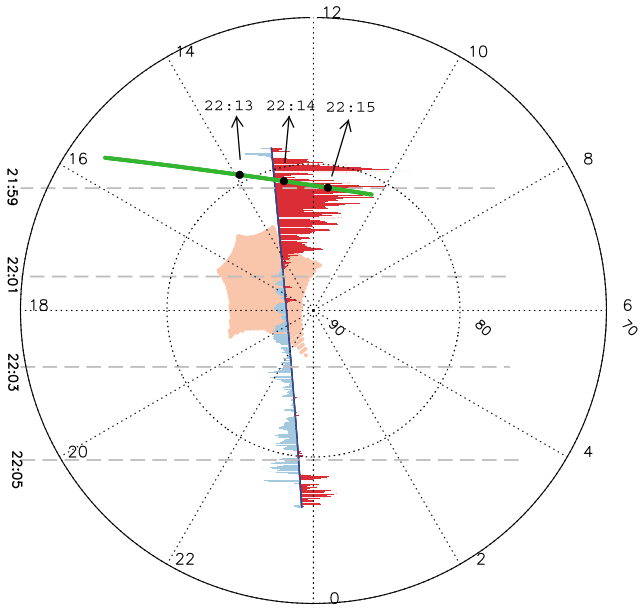

Figure 9. The e-POP and DMSP F16 satellite orbits and measurements during Event 3 on 30 May 2014, similar to Figure 2. From 21:58 to 22:06 UT, e-POP went from 78° magnetic latitude in the dayside cleft near 13 MLT into the polar cap and nightside region. From 21:58 to 22:01, the SEI encountered very large ion upflow velocities up to 3 km/s around polar cap boundary after the magnetic local noon. It should be noted that the ion data are integrated to 0.1 s to calculate the cross-track ion velocities. Immediately after the broad and strong upflow region, a weak downward flow region ensued. The largest ion downward flow velocity reached 0.9 km/s. The three times shown (22:13, 22:14 and 22:15 UT) by the black dots represent the close conjunction times of the DMSP F16 satellite. The RISR-N FOV is displayed as the salmon polygon region. Both ion and electron temperature elevations are observed by RISR-N in this case.

baseline value is 700 m/s. Immediately after the broad and strong upflow region, a weak downward flow region ensues. The largest ion downward flow velocity reaches 0.9 km/s. The ion fountain feature is clearly identifiable in this event. About 13 min later, from 22:13 to 22:15 UT, the DMSP F16 satellite (green line) traversed the intense ion upflow region. The SSJ/5 instrument onboard the satellite observed intense fluxes of both low-energy (20–300 eV) electron and ion precipitation. Also, data from RISR-N show lasting electron temperature enhancements (up to 4000 K, not shown) with small ion temperature increases (up to 0.26 eV). The *Kp* index for this event is 1+, and the IMF B_y and B_z are both relatively stable for 40 min from 21:40 to 22:20 UT (B_y is 7–9 nT, B_z is 6–9 nT).

Figure 10 summarizes the observations from the e-POP SEI and the MGF in the same manner as done previously. Figure 10a displays the ion upflow velocity profile shown in Figure 9. The intense ion upflow region spanned 3 min, representing over 1000 km in spatial scale along the spacecraft track. Figure 10b displays the perpendicular FWHM profile of ion distributions every 0.1 s. There are some weak fluctuations in the region of strong ion upflow representing an upper limit of ion heating of 0.32 eV. The magnetic field ΔB_y component, however, exhibits large perturbations up to 1000 nT in the ion upflow region, which is displayed in Figure 10c. The large and broad paired sheets are presented with some structured small currents embedded within this region. The largest ion upflow velocity is observed in the large-scale downward current region in the initial 1.5 min of the observation. Some fluctuations of ΔB_y within the large-scale downward currents are associated with the strongest ion upflow. During this time, the IRM data again indicates that O^+ ions dominate (95%) the event along with a fraction of H^+, N^+, and NO^+.

Figure 11 shows the precipitating electron and ion observations from the DMSP F16 SSJ/5 instrument for this event. The DMSP F16 satellite went across the cleft region from 22:13 to 22:14 UT as indicated within the rectangular red box, during which period the SSJ/5 observed intense soft precipitating electrons and ions, both with average energies below 100 eV and with total energy fluxes of over 10^{11} eV cm^{-2} s^{-1}. From 22:14 to 22:15 UT, the average ion energy increases to 1 KeV and then gradually decreases to less than 300 eV. Except for the less than 300 eV average ion energy, the above features are typical cusp characteristics defined in *Newell and Meng* [1989]. Figure 11d displays the magnetic field perturbation data in this case. The large perturbations

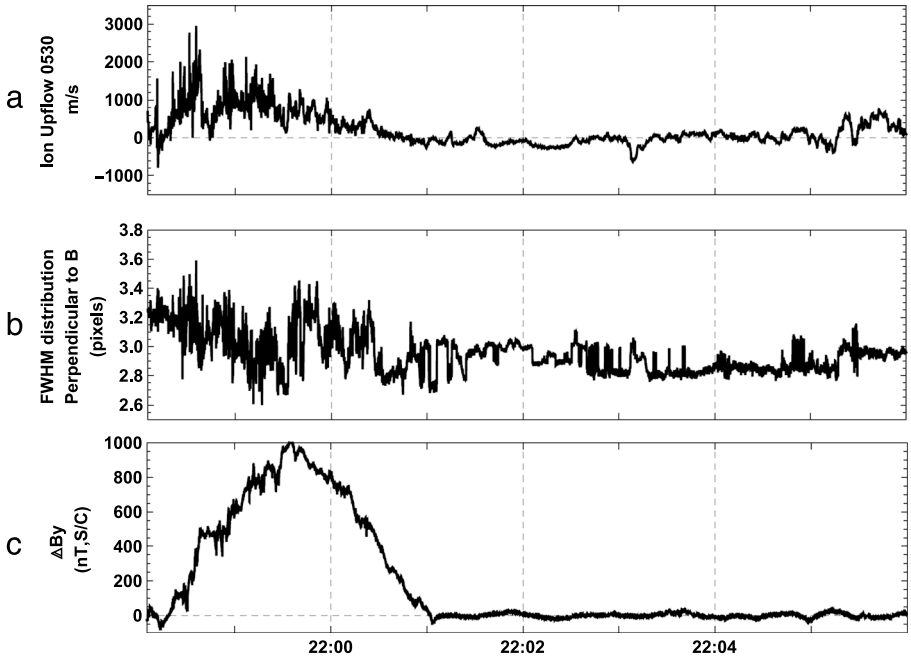

Figure 10. Observations from the e-POP SEI and the MGF for Event 3 on 30 May 2014 in the same manner as in Figure 3. (a) The ion upflow velocity profile. (b) The perpendicular FWHM profile of ion distributions every 0.1 s. There are some weak fluctuations in the region of strong ion upflow representing an upper limit of ion heating of 0.32 eV. (c) The magnetic field ΔB_y component, which exhibits large perturbations up to 1000 nT in the ion upflow region. The large and broad two-current sheets are presented with some structured small currents embedded within this region. The largest ion upflow velocity is observed in the large-scale downward current region in the initial 1.5 min of the experiment.

in both *y* and *z* directions suggest that the infinite current sheet assumption underestimates the magnitudes of FACs in this region.

Figure 12 presents the convection measurements from SuperDARN coinciding with ion upflow from 21:58 to 22:00 UT. A striking feature observed in this figure is the coincidence of a large convection vortex within the intense ion upflow region observed by the SEI. The e-POP trajectory while observing ion upflow is indicated by the red line. Near the polar cap boundary at around 80° AACGM latitude and 13 MLT there is a rotation of convection from westward to eastward around the convection vortex. This convection vortex is consistent with the positive divergence of electric fields, which, based on current continuity assumption, represents large downward currents flowing into this region [*Sofko et al.*, 1995]. This is again in agreement with the MGF observations from e-POP.

3.4. Field-Aligned Currents and Ion Upflow

In all the three events, there is a close correlation between the ion upflow velocities and currents. Field-aligned currents tend to indicate regions of enhanced particle precipitation, convective flows, and Poynting flux, and therefore serve as indirect indicators of energy input into the ion upflow process. We further quantify this relationship given the ion upflow velocities and the FACs observed in all these three events. The values are calculated in 5 s intervals. Figure 13 correlates the ion upflow velocities with the magnitudes of both downward (flowing into the ionosphere) and upward (flowing out of the ionosphere) currents. Least squares linear fitting was applied to the data with the fitted model of $Y = 64.75 + 371.00 \times \mathrm{FAC}$, where Y is the upflow velocity and FAC is the magnitude of the current. The relatively weak correlation coefficient (0.51) is perhaps not surprising given the fact that ion velocities measured at any one instant in time are the integrated effect of upward acceleration taking place over many minutes, resulting in a nonperfect alignment of the FAC and ion upflow time series. The moderate coefficient also indicates that there are factors other than large-scale DC FACs, such as precipitating electrons and small-scale AC FACs, contributing to the energy budget of ion thermal expansion. Fourier analysis of the magnetic field perturbation data and ion upflow velocities suggests some correlation between these two quantities at several hertz, which is a topic of future study.

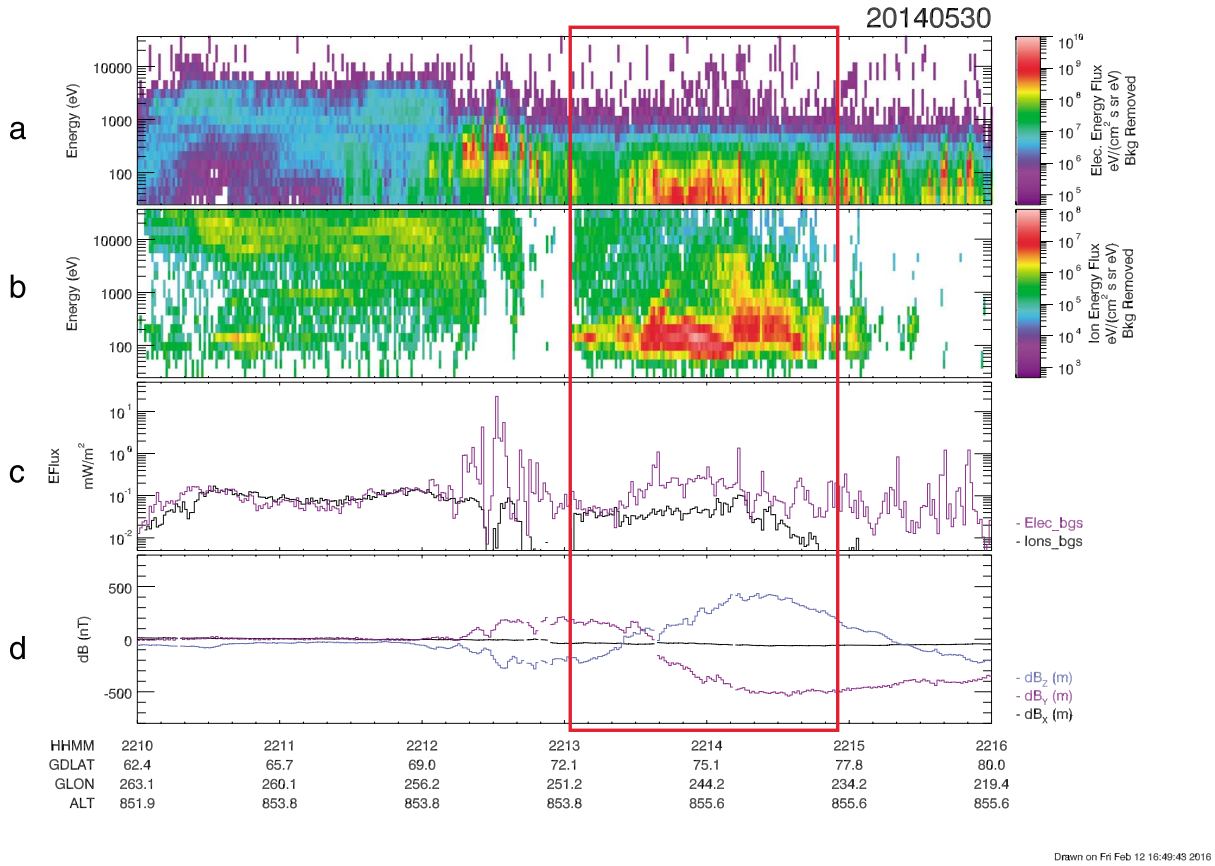

Figure 11. Precipitating electron and ion observations from the DMSP F16 in Event 3 on 30 May 2014, in the same format as Figure 4. The DMSP F16 satellite went across the cleft region from 22:13 to 22:14 UT as indicated within the rectangular red box, during which period the SSJ/5 observed intense soft precipitating electrons and ions, both with average energies below 100 eV and with total energy fluxes of over 10^{11} eV cm^{-2} s^{-1}. From 22:14 to 22:15 UT, the average ion energy increases to 1 keV and then gradually decreases to less than 300 eV. These are cusp-like particle precipitating characteristics. (d) The magnetic field perturbation data in this case. The large perturbations in both *y* and *z* directions suggest that the infinite current sheet assumption underestimates the magnitudes of FACs in this region.

4. Discussion

In this paper, we introduce three cleft ion fountain events observed by the SEI instrument onboard the e-POP satellite at around 1000 km altitude during geomagnetically quiet periods. Along with the ion upflow, we also observe large-scale multiple field-aligned current sheets to be associated with these events. For the first two events, close conjunctions with DMSP F16 satellite establish the presence of intense, soft electron precipitation accompanying the ion upflow. Also, convection data from SuperDARN reveal that for all the events in question, some degree of convection velocity gradients or, for two of the three events, convection vortices are present in the conjugate lower ionosphere.

Similar features have been reported by *Heelis et al.* [1984], *Tsunoda et al.* [1989], *Loranc et al.* [1991], and *Liu and Lu* [2004]. *Heelis et al.* [1984] reported ion upflow velocities in excess of 2 km/s in the nightside auroral region associated with very large field-aligned currents, soft electron precipitation, and convection velocity gradients and suggested that a field-aligned electric field was responsible for the upward ion acceleration. Based on HILAT satellite observations, *Tsunoda et al.* [1989] demonstrated cases where thermal ion upwelling was collocated with cleft electron precipitation, upward field-aligned currents and large convection velocity gradients or, in some events, convection reversals. They argued that velocity-shear-related energization processes were responsible for the observed ion upflow. *Loranc et al.* [1991] statistically investigated the morphology of vertical ion flows in the cusp and auroral region and found that large ion upflow velocities were generally associated with large convection speeds. They explained their results in terms of ion-neutral frictional heating leading to upward acceleration via the transient change in the ion scale height. Most of their data were sampled at low altitudes (216–400 km) with even fewer events in quiet periods ($Kp < 3$). *Liu and Lu* [2004],

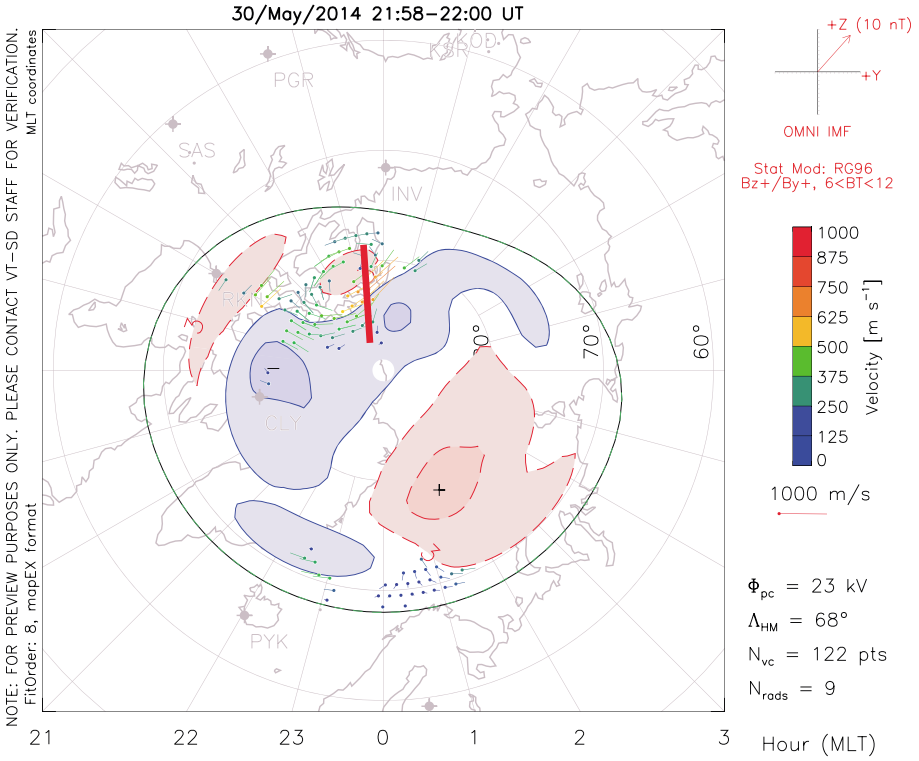

Figure 12. The 2 min averaged convection map from SuperDARN for Event 3 on 30 May 2014, in the same format as in Figure 5. A striking feature observed in this figure is the coincidence of a large convection vortex with the intense ion upflow region observed by the SEI. The e-POP trajectory while observing ion upflow is indicated by the red line. Near the polar cap boundary at around 80° and 13 MLT, there is a rotation of convection from westward to eastward around the convection vortex. This convection vortex is consistent with the positive divergence of electric fields, which represents large downward currents flowing into this region.

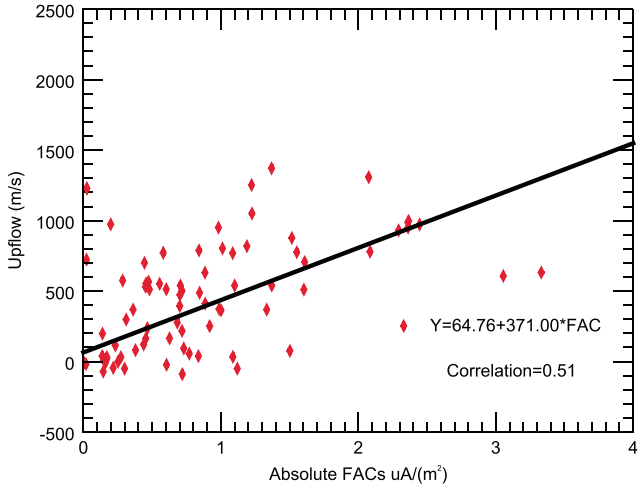

Figure 13. Fitted relationship between ion upflow and the magnitude of FACs for three events. Least squares linear fitting was applied to the data with the fitted model of $Y = 64.75 + 371.00 \times \mathrm{FAC}$, where Y is the upflow velocity and FAC is the magnitude of the current. The correlation coefficient is 0.51.

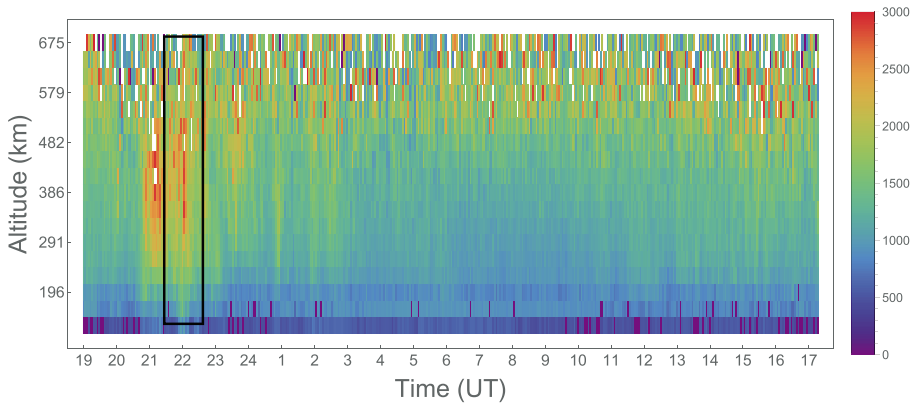

Figure 14. The 3 min integrated ion temperature altitudinal profile from RISR-N in Event 3 on 30 May 2014. The region indicated inside the black box region near 22:00 UT corresponds to the ion upflow region observed by the e-POP SEI. The upper limit of the ion heating is 3000 K (0.26 eV), which is consistent with the upper limit of ion heating of 0.32 eV observed by the SEI.

based on observations from European Incoherent Scatter (EISCAT), UVI images from the POLAR satellite and simulation results, argued that frictional heating and soft electron precipitation cannot be the cause of ion energization. Instead, they proposed ion heating driven by shear-driven instabilities to be the cause.

As mentioned in section 1, in the dayside cleft region at low altitudes, there are principally three mechanisms proposed for ion upflow, namely, frictional heating, soft electron precipitation, and ion heating via wave-particle interactions. Field-aligned currents and velocity shear instabilities [*Kindel and Kennel*, 1971; *Ganguli et al.*, 1994] are suggested to cause these plasma waves and therefore to provide the source of free energy to heat the thermal ions. In our low geomagnetic activity events ($Kp = 0+$, 2−, and 1+), as inferred from ground-based radar observations, the ion convection velocities are less than 1000 m/s in Events 1 and 2, and less than 1400 m/s in Event 3. Despite large variability, these velocities are less than the values exceeding 2 km/s reported by *Heelis et al.* [1984], *Heelis et al.* [1993], and *Lorance et al.* [1991]. Furthermore, observations of the core ion distributions from the SEI place an upper limit on the ion temperature of the order of 0.3 eV. Figures 3b, 7b, and 10b demonstrate this point. The ion temperatures derived from the SEI are further validated by the conjunctional RISR-N observations in our most intense event in 30 May 2014. Figure 14 shows the ion temperature altitudinal profiles from one of the five beams (az/el: 5.3°/60.5°). The other four beam results display features consistent with this one and are not shown. The red box region at the conjunctional period near 22:00 UT demonstrates ion (O^+) heating up to 3000 K (0.26 eV) in the *F* region ionosphere. This amount of ion heating amounts to less than 0.1 g acceleration via the mirror force and typically corresponds to ion upflow velocities of less than 1 km/s [*Wahlund et al.*, 1992; *Seo et al.*, 1997; *Ogawa et al.*, 2000]. Therefore, heating is unlikely a determinant cause of the ion upflows we observe, although it may play a role in Event 3.

Instead, we argue that, during low geomagnetic activity periods as in our cases, the observed large upflow velocities in the dayside cleft region around 1000 km are mainly the result of parallel acceleration via an ambipolar electric field established by the magnetosheath-like soft electron precipitation. Figures 4 and 11 show the presence of electron precipitation of magnetosheath-like characteristics (average energy <1 keV) coinciding with our observed ion upflows in Events 1 and 3. In addition, the conjunctional RISR-N observations in the upflow regions in Events 1 and 3 display large electron temperature enhancement (from 2000 K to over 4000 K, not shown here), which is in accord with the ambipolar upflow scenario, meaning that ions are pulled upward by electrons heated by cleft precipitation.

Similar conclusions have been made in previous studies [*Seo et al.*, 1997; *Horwitz and Moore*, 1997; *Ogawa et al.*, 2003; *Burchill et al.*, 2010]. *Liu et al.* [1995] used a dynamic fluid code to model *F* region upflows associated with soft electron precipitation and frictional heating. They suggested that an electron flux of 1 erg cm^{-2} s^{-1} with characteristic energy of 150 eV can produce a 10^9 cm^{-2} s^{-1} O^+ upflow flux at 700–800 km. That is, approximately, soft electron precipitation energy fluxes of the order of 10^{11} eV cm^{-2} s^{-1} can produce O^+ ion upflow fluxes of the order of 10^9 cm^{-2} s^{-1}. In Event 1, the characteristic energies range from 50 eV to about 500 eV with peak energy fluxes of over 1 mW m^{-2} (1 erg cm^{-2} s^{-1}) as indicated by Figure 4c. Observations from the SEI reveal that the average ion upflow velocity during this event was about 700 m/s. Given that we fit a Chap-

man profile based on RISR-N density data and extrapolate a density value of 1.25×10^4 cm^{-3} at 1000 km, the ion flux is about 0.875×10^9 cm^{-2} s^{-1}.

Seo et al. [1997] and *Su et al.* [1999] found that there is an inverse relationship between upward O^+ fluxes and the characteristic energy of precipitating electrons and that precipitating electrons having energies of the order of and lower than 100 eV are more efficient in heating thermal electrons than those with higher characteristic energy. Based on SIERRA sounding rocket measurements both in the nightside auroral zone and in the dayside cusp/cleft, *Lynch et al.* [2007] and *Frederick-Frost et al.* [2007] suggested that soft electron precipitation with energy lower than 100 eV appears to be the trigger of the observed ion upflow. In Event 3, the soft electron precipitation peak energy fluxes are over 10^{11} eV cm^{-2} s^{-1} with average energies less than 100 eV.

Knudsen et al. [1998] found that the core ion heating is associated with a threshold level of electron flux of the order of 10^7 cm^{-2} s^{-1} for electron energies lower than 1 keV during active conditions ($Kp > 4$). In the present study we find no evidence of core heating in the presence of electron fluxes exceeding 10^8 cm^{-2} s^{-1}, though at much lower activity levels. This suggests that ion heating is controlled by parameters other than, or perhaps in addition to, soft electron flux.

5. Conclusion

1. Based on observations from e-POP at about 1000 km altitude during quiet geomagnetic activity, we introduce three cleft ion fountain events with large ion upflow velocities (>1.6 km/s), the magnitudes of which are comparable with those reported previously during active periods. O^+ ions dominate (90%) these events with a fraction (10%) of H^+ and other ions.
2. Large-scale field-aligned current sheets and convection velocity gradients accompany these ion upflow events. The most intense ion upflows are associated with downward current regions. For one particular event, these downward currents are embedded within a large upward current region.
3. The moderate correlation coefficient (0.51) between upflow velocities and currents implies that FACs serve as indirect energy inputs to the ion upflow process.
4. Analysis of the core ion distribution images from the e-POP SEI demonstrate that despite the large upflow velocities, the ion temperature within the cleft ion fountain does not rise by more than 0.3 eV relative to background values, which is consistent with RISR-N observations at lower altitudes. The presence of intense soft electron precipitation seen by DMSP and lack of strong ion heating both perpendicular and parallel to B indicate that the ion upflows within the dayside cleft ion fountain near 1000 km during quiet times ($Kp < 3$) are primarily driven by ambipolar electric fields.

Acknowledgments
This work was supported by an Eyes High Doctoral Recruitment Scholarship from University of Calgary and the Natural Sciences and Engineering Research Council of Canada (NSERC). e-POP is funded by the Canadian Space Agency. David M. Miles is supported by an NSERC PGS-D doctoral scholarship. Acknowledgments are owing to GeoForschungsZentrum (GFZ) Potsdam and World Data Center (WDC) for Geomagnetism, Kyoto for providing the *Kp* index; OMNI database for providing the IMF data. The authors acknowledge the use of SuperDARN data. SuperDARN is a collection of radars funded by national scientific funding agencies of Australia, Canada, China, France, Japan, South Africa, United Kingdom, and the United States of America. The Canadian SuperDARN radars are operated by the University of Saskatchewan and are supported by the Canadian Space Agency's Geospace Observatory (GO) program and the Canada Foundation for Innovation's Major Science Initiatives (CFI MSI) program.

References

André, M., and A. Yau (1997), Theories and observations of ion energization and outflow in the high latitude magnetosphere, *Space Sci. Rev.*, *80*(1–2), 27–48, doi:10.1023/A:1004921619885.

André, M., G. B. Crew, W. K. Peterson, A. M. Persoon, C. J. Pollock, and M. J. Engebretson (1990), Ion heating by broadband low-frequency waves in the cusp/cleft, *J. Geophys. Res.*, *95*(A12), 20,809–20,823, doi:10.1029/JA095iA12p20809.

André, M., P. Norqvist, A. Vaivads, L. Eliasson, O. Norberg, A. I. Eriksson, and B. Holback (1994), Transverse ion energization and wave emissions observed by the Freja satellite, *Geophys. Res. Lett.*, *21*(17), 1915–1918, doi:10.1029/94GL00699.

Bahcivan, H., R. Tsunoda, M. Nicolls, and C. Heinselman (2010), Initial ionospheric observations made by the new Resolute incoherent scatter radar and comparison to solar wind IMF, *Geophys. Res. Lett.*, *37*, L15103, doi:10.1029/2010GL043632.

Bouhram, M., B. Klecker, W. Miyake, H. Rème, J.-A. Sauvaud, M. Malingre, L. Kistler, and A. Blagau (2004), On the altitude dependence of transversely heated O^+ distributions in the cusp/cleft, *Ann. Geophys.*, *22*(5), 1787–1798.

Burchill, J. K., D. J. Knudsen, B. J. J. Bock, R. F. Pfaff, D. D. Wallis, J. H. Clemmons, S. R. Bounds, and H. Stenbaek-Nielsen (2004), Core ion interactions with BB ELF, lower hybrid, and Alfvén waves in the high-latitude topside ionosphere, *J. Geophys. Res.*, *109*, A01219, doi:10.1029/2003JA010073.

Burchill, J. K., D. J. Knudsen, J. H. Clemmons, K. Oksavik, R. F. Pfaff, C. T. Steigies, A. W. Yau, and T. K. Yeoman (2010), Thermal ion upflow in the cusp ionosphere and its dependence on soft electron energy flux, *J. Geophys. Res.*, *115*, A05206, doi:10.1029/2009JA015006.

Chappell, C. R. (1988), The terrestrial plasma source: A new perspective in solar-terrestrial processes from Dynamics Explorer, *Rev. Geophys.*, *26*(2), 229–248, doi:10.1029/RG0210.1029/RG026i002p002296i002p00229.

Chappell, C. R., S. A. Fields, C. Baugher, J. H. Hoffman, W. B. Hanson, W. W. Wright, H. D. Hammack, G. R. Carignan, and A. F. Nagy (1981), The retarding ion mass spectrometer on Dynamics Explorer-A, *Space Sci. Instrum.*, *5*, 477–491.

Cogger, L., et al. (2015), Fast auroral imager (FAI) for the e-POP mission, *Space Sci. Rev.*, *189*(1–4), 15–25, doi:10.1007/s11214-014-0107-x.

Endo, M., R. Fujii, Y. Ogawa, S. Buchert, S. Nozawa, S. Watanabe, and N. Yoshida (2000), Ion upflow and downflow at the topside ionosphere observed by the EISCAT VHF radar, *Ann. Geophys.*, *18*(2), 170–181, doi:10.1007/s00585-000-0170-3.

Fernandes, P. A., et al. (2016), Measuring the seeds of ion outflow: Auroral sounding rocket observations of low-altitude ion heating and circulation, *J. Geophys. Res. Space Physics*, *121*, 1587–1607, doi:10.1002/2015JA021536.

Frank, L. A., K. L. Ackerson, and D. M. Yeager (1977), Observations of atomic oxygen O^+) in the Earth's magnetotail, *J. Geophys. Res.*, *82*(1), 129–134, doi:10.1029/JA082i001p00129.

Frederick-Frost, K. M., K. A. Lynch, P. M. Kintner, E. Klatt, D. Lorentzen, J. Moen, Y. Ogawa, and M. Widholm (2007), SERSIO: Svalbard EISCAT rocket study of ion outflows, *J. Geophys. Res.*, *112*, A08307, doi:10.1029/2006JA011942.

Ganguli, G., M. J. Keskinen, H. Romero, R. Heelis, T. Moore, and C. Pollock (1994), Coupling of microprocesses and macroprocesses due to velocity shear: An application to the low-altitude ionosphere, *J. Geophys. Res.*, *99*(A5), 8873–8889, doi:10.1029/93JA03181.

Hardy, D. A., E. G. Holeman, W. J. Burke, L. C. Gentile, and K. H. Bounar (2008), Probability distributions of electron precipitation at high magnetic latitudes, *J Geophys. Res.*, *113*, A06305, doi:10.1029/2007JA012746.

Heelis, R. A., J. D. Winningham, M. Sugiura, and N. C. Maynard (1984), Particle acceleration parallel and perpendicular to the magnetic field observed by DE-2, *J. Geophys. Res.*, *89*(A6), 3893–3902, doi:10.1029/JA089iA06p03893.

Heelis, R. A., G. J. Bailey, R. Sellek, R. J. Moffett, and B. Jenkins (1993), Field-aligned drifts in subauroral ion drift events, *J. Geophys. Res.*, *98*(A12), 21,493–21,499, doi:10.1029/93JA02209.

Heikkila, W. J. (1985), Definition of the Cusp, in *The Polar Cusp, NATO ASI Ser.*, vol. 145, edited by J. A. Holtet and A. Egeland, pp. 387–395, Springer, Netherlands, doi:10.1007/978-94-009-5295-9_28.

Heikkila, W. J., and J. D. Winningham (1971), Penetration of magnetosheath plasma to low altitudes through the dayside magnetospheric cusps, *J. Geophys. Res.*, *76*(4), 883–891, doi:10.1029/JA076i004p00883.

Heinselman, C. J., and M. J. Nicolls (2008), A Bayesian approach to electric field and E-region neutral wind estimation with the Poker Flat Advanced Modular Incoherent Scatter Radar, *Radio Sci.*, *43*, RS5013, doi:10.1029/2007RS003805.

Horwitz, J., and T. Moore (1997), Four contemporary issues concerning ionospheric plasma flow to the magnetosphere, in *Transport Across the Boundaries of the Magnetosphere, Space Science Series of ISSI*, vol. 2, edited by B. Hultqvist and M. Øieroset, pp. 49–76, Springer, Netherlands, doi:10.1007/978-94-009-0045-5_3.

Horwitz, J. L., and M. Lockwood (1985), The cleft ion fountain: A two-dimensional kinetic model, *J. Geophys. Res.*, *90*(A0), 9749–9762, doi:10.1029/JA090iA10p09749.

Johnson, R. G., R. D. Sharp, and E. G. Shelley (1977), Observations of ions of ionospheric origin in the storm-time ring current, *Geophys. Res. Lett.*, *4*(10), 403–406, doi:10.1029/GL004i010p00403.

Kervalishvili, G. N., and H. Lühr (2013), The relationship of thermospheric density anomaly with electron temperature, small-scale FAC, and ion up-flow in the cusp region, as observed by CHAMP and DMSP satellites, *Ann. Geophys.*, *31*(3), 541–554, doi:10.5194/angeo-31-541-2013.

Khazanov, G. V., M. W. Liemohn, and T. E. Moore (1997), Photoelectron effects on the self-consistent potential in the collisionless polar wind, *J. Geophys. Res.*, *102*(A4), 7509–7521, doi:10.1029/96JA03343.

Kindel, J. M., and C. F. Kennel (1971), Topside current instabilities, *J. Geophys. Res.*, *76*(13), 3055–3078, doi:10.1029/JA076i013p03055.

Knudsen, D., J. Burchill, T. Cameron, G. Enno, A. Howarth, and A. Yau (2015), The CASSIOPE/e-POP suprathermal electron imager (SEI), *Space Sci. Rev.*, *189*(1–4), 65–78, doi:10.1007/s11214-015-0151-1.

Knudsen, D. J., B. A. Whalen, T. Abe, and A. Yau (1994), Temporal evolution and spatial dispersion of ion conics: Evidence for a polar cusp heating wall, in *Solar System Plasmas in Space and Time*, edited by J. L. Burch and J. H. Waite, pp. 163–169, AGU, Washington, D. C., doi:10.1029/GM084p0163.

Knudsen, D. J., J. H. Clemmons, and J.-E. Wahlund (1998), Correlation between core ion energization, suprathermal electron bursts, and broadband ELF plasma waves, *J. Geophys. Res.*, *103*(A3), 4171–4186, doi:10.1029/97JA00696.

Liu, C., J. L. Horwitz, and P. G. Richards (1995), Effects of frictional ion heating and soft-electron precipitation on high-latitude F-region upflows, *Geophys. Res. Lett.*, *22*(20), 2713–2716, doi:10.1029/95GL02551.

Liu, H., and G. Lu (2004), Velocity shear-related ion upflow in the low-altitude ionosphere, *Ann. Geophys.*, *22*(4), 1149–1153, doi:10.5194/angeo-22-1149-2004.

Lockwood, M., J. H. Waite, T. E. Moore, J. F. E. Johnson, and C. R. Chappell (1985a), A new source of suprathermal O^+ ions near the dayside polar cap boundary, *J. Geophys. Res.*, *90*(A5), 4099–4116, doi:10.1029/JA090iA05p04099.

Lockwood, M., M. O. Chandler, J. L. Horwitz, J. H. Waite, T. E. Moore, and C. R. Chappell (1985b), The cleft ion fountain, *J. Geophys. Res.*, *90*(A10), 9736–9748, doi:10.1029/JA090iA10p09736.

Loranc, M., and J. P. St.-Maurice (1994), A time-dependent gyro-kinetic model of thermal ion upflows in the high-latitude F region, *J. Geophys. Res.*, *99*(A9), 17,429–17,451, doi:10.1029/93JA01852.

Loranc, M., W. B. Hanson, R. A. Heelis, and J.-P. St.-Maurice (1991), A morphological study of vertical ionospheric flows in the high-latitude F region, *J. Geophys. Res.*, *96*(A3), 3627–3646, doi:10.1029/90JA02242.

Lühr, H., J. Park, J. W. Gjerloev, J. Rauberg, I. Michaelis, J. M. G. Merayo, and P. Brauer (2015), Field-aligned currents' scale analysis performed with the Swarm constellation, *Geophys. Res. Lett.*, *42*, 1–8, doi:10.1002/2014GL062453.

Lundin, R., I. Sandahl, B. Hultqvist, A. Galeev, O. Likhin, A. Omelchenko, N. Pissarenko, O. Vaisberg, and A. Zacharov (1979), First observations of the hot ion composition in the high altitude magnetospheric boundary layer by means of Prognoz-7, ESA SP-148 presented at Magnetospheric Boundary Layers Conference, pp. 91–96, Alpbach, 11–15 Jun.

Lynch, K. A., J. L. Semeter, M. Zettergren, P. Kintner, R. Arnoldy, E. Klatt, J. LaBelle, R. G. Michell, E. A. MacDonald, and M. Samara (2007), Auroral ion outflow: Low altitude energization, *Ann. Geophys.*, *25*(9), 1967–1977, doi:10.5194/angeo-25-1967-2007.

Moore, T. E., C. R. Chappell, M. Lockwood, and J. H. Waite (1985), Superthermal ion signatures of auroral acceleration processes, *J. Geophys. Res.*, *90*(A2), 1611–1618, doi:10.1029/JA090iA02p01611.

Moore, T. E., C. J. Pollock, M. L. Adrian, P. M. Kintner, R. L. Arnoldy, K. A. Lynch, and J. A. Holtet (1996), The cleft ion plasma environment at low solar activity, *Geophys. Res. Lett.*, *23*(14), 1877–1880, doi:10.1029/96GL00843.

Moore, T. E., M.-C. Fok, D. C. Delcourt, S. P. Slinker, and J. A. Fedder (2010), Global response to local ionospheric mass ejection, *J. Geophys. Res.*, *115*, A00J14, doi:10.1029/2010JA015640.

Newell, P. T., and C.-I. Meng (1989), On quantifying the distinctions between the cusp and the CLEFT/LLBL, in *Electromagnetic Coupling in the Polar Clefts and Caps, NATO ASI Ser.*, vol. *278*, edited by P. E. Sandholt and A. Egeland, pp. 87–101, Springer, Netherlands, doi:10.1007/978-94-009-0979-3_6.

Norqvist, P., M. André, L. Eliasson, A. I. Eriksson, L. Blomberg, H. Lühr, and J. H. Clemmons (1996), Ion cyclotron heating in the dayside magnetosphere, *J. Geophys. Res.*, *101*(A6), 13,179–13,193, doi:10.1029/95JA03596.

Ogawa, Y., R. Fujii, S. C. Buchert, S. Nozawa, S. Watanabe, and A. P. van Eyken (2000), Simultaneous EISCAT Svalbard and VHF radar observations of ion upflows at different aspect angles, *Geophys. Res. Lett.*, *27*(1), 81–84, doi:10.1029/1999GL010665.

Ogawa, Y., R. Fujii, S. C. Buchert, S. Nozawa, and S. Ohtani (2003), Simultaneous EISCAT Svalbard radar and DMSP observations of ion upflow in the dayside polar ionosphere, *J. Geophys. Res.*, *108*(A3), 1101, doi:10.1029/2002JA009590.

Ogawa, Y., et al. (2008), Coordinated EISCAT Svalbard radar and Reimei satellite observations of ion upflows and suprathermal ions, *J. Geophys. Res.*, *113*, A05306, doi:10.1029/2007JA012791.

Peterson, W. K., R. D. Sharp, E. G. Shelley, R. G. Johnson, and H. Balsiger (1981), Energetic ion composition of the plasma sheet, *J. Geophys. Res.*, *86*(A2), 761–767, doi:10.1029/JA086iA02p00761.

Pollock, C. J., M. O. Chandler, T. E. Moore, J. H. Waite, C. R. Chappell, and D. A. Gurnett (1990), A survey of upwelling ion event characteristics, *J. Geophys. Res.*, *95*(A11), 18,969–18,980, doi:10.1029/JA095iA11p18969.

Redmon, R. J. (2014), DMSP space Wx SSJ, SSM, SSIES ATBD and user's manual, version 1.0, Tech. Rep., Natl. Cent. for Environ. Inf., Asheville, NC.

Rich, F. J., M. Gussenhoven, and M. E. Greenspan (1987), Using simultaneous particle and field observations on a low-altitude satellite to estimate Joule heat energy flow into the high-latitude ionosphere, Tech. Rep., Air Force Geophys. Lab., Hanscom AFB, Mass.

Roth, I., and M. K. Hudson (1985), Lower hybrid heating of ionospheric ions due to ion ring distributions in the cusp, *J. Geophys. Res.*, *90*(A5), 4191–4203, doi:10.1029/JA090iA05p04191.

Ruohoniemi, J. M., and K. B. Baker (1998), Large-scale imaging of high-latitude convection with Super Dual Auroral Radar Network HF radar observations, *J. Geophys. Res.*, *103*(A9), 20,797–20,811, doi:10.1029/98JA01288.

Sangalli, L., D. J. Knudsen, M. F. Larsen, T. Zhan, R. F. Pfaff, and D. Rowland (2009), Rocket-based measurements of ion velocity, neutral wind, and electric field in the collisional transition region of the auroral ionosphere, *J. Geophys. Res.*, *114*, A04306, doi:10.1029/2008JA013757.

Seo, Y., J. L. Horwitz, and R. Caton (1997), Statistical relationships between high-latitude ionospheric F region/topside upflows and their drivers: DE 2 observations, *J. Geophys. Res.*, *102*(A4), 7493–7500.

Shelley, E., D. Simpson, T. Sanders, E. Hertzberg, H. Balsiger, and A. Ghielmetti (1981), The energetic ion composition spectrometer/EICS/for the Dynamics Explorer-A, *Space Sci. Instrum.*, *5*, 443–454.

Shelley, E. G., R. G. Johnson, and R. D. Sharp (1972), Satellite observations of energetic heavy ions during a geomagnetic storm, *J. Geophys. Res.*, *77*(31), 6104–6110, doi:10.1029/JA077i031p06104.

Skjæveland, Å., J. Moen, and H. C. Carlson (2014), Which cusp upflow events can possibly turn into outflows?, *J. Geophys. Res. Space Physics*, *119*, 6876–6890, doi:10.1002/2013JA019495.

Sofko, G. J., R. Greenwald, and W. Bristow (1995), Direct determination of large-scale magnetospheric field-aligned currents with SuperDARN, *Geophys. Res. Lett.*, *22*(15), 2041–2044, doi:10.1029/95GL01317.

Strangeway, R. J., R. E. Ergun, Y.-J. Su, C. W. Carlson, and R. C. Elphic (2005), Factors controlling ionospheric outflows as observed at intermediate altitudes, *J. Geophys. Res.*, *110*, A03221, doi:10.1029/2004JA010829.

Su, Y.-J., R. G. Caton, J. L. Horwitz, and P. G. Richards (1999), Systematic modeling of soft-electron precipitation effects on high-latitude F region and topside ionospheric upflows, *J. Geophys. Res.*, *104*(A1), 153–163, doi:10.1029/1998JA900068.

Tam, S. W. Y., F. Yasseen, T. Chang, and S. B. Ganguli (1995), Self-consistent kinetic photoelectron effects on the polar wind, *Geophys. Res. Lett.*, *22*(16), 2107–2110, doi:10.1029/95GL01846.

Tsunoda, R. T., R. C. Livingston, J. F. Vickrey, R. A. Heelis, W. B. Hanson, F. J. Rich, and P. F. Bythrow (1989), Dayside observations of thermal-ion upwellings at 800-km altitude: An ionospheric signature of the cleft ion fountain, *J. Geophys. Res.*, *94*(A11), 15,277–15,290, doi:10.1029/JA094iA11p15277.

Wahlund, J. E., H. J. Opgenoorth, I. Häggström, K. J. Winser, and G. O. L. Jones (1992), Eiscat observations of topside ionospheric ion outflows during auroral activity: Revisited, *J Geophys. Res.*, *97*(A3), 3019–3037, doi:10.1029/91JA02438.

Waite, J. H., T. Nagai, J. F. E. Johnson, C. R. Chappell, J. L. Burch, T. L. Killeen, P. B. Hays, G. R. Carignan, W. K. Peterson, and E. G. Shelley (1985), Escape of suprathermal O^+ ions in the polar cap, *J. Geophys. Res.*, *90*(A2), 1619–1630, doi:10.1029/JA090iA02p01619.

Waite, J. H., T. E. Moore, M. O. Chandler, M. Lockwood, A. Persoon, and M. Suguira (1986), Ion energization in upwelling ion events, in *Ion Acceleration in the Magnetosphere and Ionosphere*, edited by T. Chang et al., pp. 61–66, AGU, Washington, D. C., doi:10.1029/GM038p0061.

Wallis, D., D. Miles, B. Narod, J. Bennest, K. Murphy, I. Mann, and A. Yau (2015), The CASSIOPE/e-POP magnetic field instrument (MGF), *Space Sci. Rev.*, *189*(1–4), 27–39, doi:10.1007/s11214-014-0105-z.

Whitteker, J. (1977), The transient response of the topside ionosphere to precipitation, *Planet. Space Sci.*, *25*(8), 773–786, doi:10.1016/0032-0633(77)90129-5.

Wilson, G. R. (1994), Kinetic modeling of O^+ upflows resulting from $E \times B$ convection heating in the high-latitude F region ionosphere, *J. Geophys. Res.*, *99*(A9), 17,453–17,466, doi:10.1029/94JA01214.

Yau, A., A. Howarth, A. White, G. Enno, and P. Amerl (2015), Imaging and rapid-scanning ion mass spectrometer (IRM) for the CASSIOPE e-POP mission, *Space Sci. Rev.*, *189*(1–4), 41–63, doi:10.1007/s11214-015-0149-8.

Yau, A. W., P. H. Beckwith, W. K. Peterson, and E. G. Shelley (1985), Long-term (solar cycle) and seasonal variations of upflowing ionospheric ion events at DE 1 altitudes, *J. Geophys. Res.*, *90*(A7), 6395–6407, doi:10.1029/JA090iA07p06395.

Yeh, H.-C., and J. C. Foster (1990), Storm time heavy ion outflow at mid-latitude, *J. Geophys. Res.*, *95*(A6), 7881–7891, doi:10.1029/JA095iA06p07881.